Microscopic calculation of the interaction cross section for stable and unstable nuclei based on the nonrelativistic nucleon-nucleon *t* matrix

Dao T. Khoa* and Hoang Sy Than
Institute for Nuclear Science & Technique, VAEC, P. O. Box 5T-160, Nghia Do, Hanoi, Vietnam

Tran Hoai Nam
Department of Physics, Hanoi University of Natural Sciences, 334 Nguyen Trai Street, Thanh Xuan, Hanoi, Vietnam

Marcella Grasso and Nguyen Van Giai
Institut de Physique Nucléaire, IN2P3-CNRS, 91406 Orsay Cedex, France
(Received 1 August 2003; published 19 April 2004)

Fully quantal calculations of the total reaction cross sections σ_R and interaction cross sections σ_I, induced by stable and unstable He, Li, C, and O isotopes on ^{12}C target at $E_{lab} \approx 0.8$ and 1 GeV/nucleon have been performed, for the first time, in the distorted wave impulse approximation (DWIA) using the microscopic *complex* optical potential and inelastic form factors given by the folding model. Realistic nuclear densities for the projectiles and ^{12}C target as well as the complex *t*-matrix parametrization of free nucleon-nucleon interaction by Franey and Love were used as inputs of the folding calculation. Our *parameter-free* folding + DWIA approach has been shown to give a very good account (within 1–2%) of the experimental σ_I measured at these energies for the stable, strongly bound isotopes. With the antisymmetrization of the dinuclear system properly taken into account, this microscopic approach is shown to be more accurate than the simple optical limit of Glauber model that was widely used to infer the nuclear radii from the measured σ_I. Therefore, the results obtained for the nuclear radii of neutron-rich isotopes under study can be of interest for further nuclear structure studies.

DOI: 10.1103/PhysRevC.69.044605 PACS number(s): 24.10.Eq, 24.10.Ht, 24.50.+g, 25.60.Bx

I. INTRODUCTION

Since 1980s the radioactive ion beams have been used intensively to measure the total reaction cross sections and interaction cross sections induced by unstable nuclei on stable targets (see a recent review in Ref. [1]) which serve as an important data bank for the determination of nuclear sizes. The discovery of exotic structures of unstable nuclei, such as neutron halos or neutron skins, are among the most fascinating results of this study.

The theoretical tool used dominantly by now to analyze the interaction cross sections measured at energies of several hundred MeV/nucleon is the Glauber model [2,3] which is based on the eikonal approximation. This approach provides a simple connection between the ground state densities of the two colliding nuclei and the total reaction cross section of the nucleus-nucleus system, and has been used, in particular, to deduce the nuclear density parameters for the neutron-rich halo nuclei [4].

In general, the total reaction cross section σ_R, which measures the loss of flux from the elastic channel, must be calculated from the transmission coefficient T_l as

$$\sigma_R = \frac{\pi}{k^2} \sum_l (2l+1) T_l, \tag{1}$$

where k is the relative momentum (or wave number). The summation is carried over all partial waves l with T_l determined from the elastic S matrix as

$$T_l = 1 - |S_l|^2. \tag{2}$$

In the standard optical model (OM), the quantal S-matrix elements S_l are obtained from the solution of the Schrödinger equation for elastic nucleus-nucleus scattering using a *complex* optical potential. At low energies, the eikonal approximation is less accurate and, instead of Glauber model, the OM should be used to calculate σ_R for a reliable comparison with the data. At energies approaching 1 GeV/nucleon region, there are very few elastic scattering data available and the choice of a realistic optical potential becomes technically difficult, especially for unstable nuclei. Perhaps, this is the reason why different versions of Glauber model are widely used to calculate σ_R at high energies. Depending on the structure model for the nuclear wave functions used in the calculation, those Glauber model calculations can be divided into two groups: the calculations using a simple optical limit of Glauber model (see Ref. [1] and references therein) and the more advanced approaches where the few-body correlation and/or breakup of a loosely bound projectile into a core and valence (halo) nucleons are treated explicitly [3,5,6].

In the present work, we explore the applicability of the standard OM to calculate the total reaction cross section (1) induced by stable and unstable beams at high energies using the microscopic optical potential predicted by the folding model. The basic inputs of a folding calculation are the densities of the two colliding nuclei and the effective nucleon-nucleon (*NN*) interaction [7]. At low energies, a realistic density-dependent *NN* interaction [8] based on the M3Y in-

*Electronic address: khoa@vaec.gov.vn

teraction [9] has been successfully used to calculate the α-nucleus and nucleus-nucleus optical potential [10]. This interaction fails, however, to predict the shape of the α-nucleus optical potential as the bombarding energy increases to about 340 MeV/nucleon [11]. On the other hand, at incident energies approaching a few hundred MeV/nucleon the *t*-matrix parametrization of free *NN* interaction was often used in the folding analysis of proton-nucleus scattering [12,13]. The use of the *t*-matrix interaction corresponds to the so-called *impulse approximation* (IA), where the medium modifications of the *NN* interaction are neglected [14].

In the present folding calculation we adopt a local representation of the free *NN t* matrix developed by Franey and Love [13] based on the experimental *NN* phase shifts. The folded optical potentials and inelastic form factors are used further in the distorted wave impulse approximation (DWIA) to calculate $\sigma_{\rm R}$ and interaction cross section $\sigma_{\rm I}$, induced by stable and unstable He, Li, C, and O isotopes on ^{12}C target at bombarding energies around 0.8 and 1 GeV/nucleon. Since relativistic effects are significant at high energies, the relativistic kinematics are taken into account properly in both the folding and DWIA calculations. To clarify the adequacy and possible limitation of the present folding model, we also discuss the main approximations made in our approach and compare them with those usually assumed in the Glauber model.

Given the realistic nuclear densities and validity of IA, the folding approach presented below in Sec. II is actually parameter-free and it is necessary to test first the reliability of the model by studying the known stable nuclei before going to study unstable nuclei. Such a procedure is discussed briefly in Sec. III. Then, $\sigma_{\rm I}$ measured for the neutron-rich He, Li, C, and O isotopes are compared with the results of calculation and the sensitivity of nuclear radii to the calculated $\sigma_{\rm I}$ is discussed. The discrepancy between $\sigma_{\rm I}^{\rm calc}$ and $\sigma_{\rm I}^{\rm expt}$ found for some light halo nuclei is discussed in detail to indicate possible effects caused by the dynamic few-body correlation. Conclusions are drawn in Sec. IV.

II. FOLDING MODEL FOR THE COMPLEX NUCLEUS-NUCLEUS OPTICAL POTENTIAL

The details of the latest double-folding formalism are given in Ref. [10] and we only recall briefly its main features. In general, the projectile-target interaction potential can be evaluated as an energy-dependent Hartree-Fock-type potential of the dinuclear system:

$$U=\sum_{i\in a,j\in A}[\langle ij|v_{\rm D}|ij\rangle+\langle ij|v_{\rm EX}|ji\rangle]=V_{\rm D}+V_{\rm EX}, \qquad (3)$$

where the nuclear interaction V is a sum of effective *NN* interactions v_{ij} between nucleon i in the projectile a and nucleon j in the target A. The antisymmetrization of the dinuclear system is done by taking into account the single-nucleon knock-on exchanges.

The direct part of the potential is local (provided that the *NN* interaction itself is local), and can be written in terms of the one-body densities,

$$V_{\rm D}(E,\boldsymbol{R})=\int \rho_a(\boldsymbol{r}_a)\rho_A(\boldsymbol{r}_A)v_{\rm D}(E,\rho,s)d^3r_a d^3r_A,$$
$$\text{where } \boldsymbol{s}=\boldsymbol{r}_A-\boldsymbol{r}_a+\boldsymbol{R}. \qquad (4)$$

The exchange part is, in general, nonlocal. However, an accurate local approximation can be obtained by treating the relative motion locally as a plane wave [15]:

$$V_{\rm EX}(E,\boldsymbol{R})=\int \rho_a(\boldsymbol{r}_a,\boldsymbol{r}_a+\boldsymbol{s})\rho_A(\boldsymbol{r}_A,\boldsymbol{r}_A-\mathbf{s})\times v_{\rm EX}(E,\rho,s)\exp\left(\frac{i\boldsymbol{K}(E,\boldsymbol{R})\cdot\boldsymbol{s}}{M}\right)d^3r_a d^3r_A. \qquad (5)$$

Here $\rho_a(\boldsymbol{r}_a)\equiv\rho_a(\boldsymbol{r}_a,\boldsymbol{r}_a)$ and $\rho_a(\boldsymbol{r}_a,\boldsymbol{r}_a+\boldsymbol{s})$ are the diagonal and nondiagonal parts of the one-body density matrix for the projectile, and similarly for the target. $\boldsymbol{K}(E,\boldsymbol{R})$ is the local momentum of relative motion determined as

$$K^2(E,\boldsymbol{R})=\frac{2\mu}{\hbar^2}[E_{\rm c.m.}-{\rm Re}\ U(E,\boldsymbol{R})-V_{\rm C}(\boldsymbol{R})], \qquad (6)$$

μ is the reduced mass, $M=aA/(a+A)$ with a and A the mass numbers of the projectile and target, respectively. Here, $U(E,\boldsymbol{R})=V_{\rm D}(E,\boldsymbol{R})+V_{\rm EX}(E,\boldsymbol{R})$ and $V_{\rm C}(\boldsymbol{R})$ are the total nuclear and Coulomb potentials, respectively. More details on the calculation of the direct and exchange potentials (4) and (5) can be found in Refs. [10,16]. The folding inputs for mass numbers and incident energies were taken as given by the relativistically corrected kinematics [17].

To calculate consistently both the optical potential and inelastic form factor one needs to take into account explicitly the multipole decomposition of the nuclear density that enters the folding calculation [10]:

$$\rho_{JM\to J'M'}(\boldsymbol{r})=\sum_{\lambda\mu}\langle JM\lambda\mu|J'M'\rangle C_\lambda\rho_\lambda(r)[i^\lambda Y_{\lambda\mu}(\hat{\boldsymbol{r}})]^*, \qquad (7)$$

where JM and $J'M'$ are the nuclear spin and its projection in the initial and final states, respectively, and $\rho_\lambda(r)$ is the nuclear transition density for the corresponding 2^λ-pole excitation. In the present work, we adopt the collective-model Bohr-Mottelson prescription [18] to construct the nuclear transition density for a given excitation in the ^{12}C target as

$$\rho_\lambda(r)=-\delta_\lambda\frac{d\rho_0(r)}{dr}. \qquad (8)$$

Here $\rho_0(r)$ is the total ground state (g.s.) density and δ_λ is the deformation length of the 2^λ-pole excitation in the ^{12}C target.

A. Impulse approximation and the *t*-matrix interaction

If the total spin and isospin are zero for one of the two colliding nuclei (^{12}C in our case) only the spin- and isospin-independent components of the central *NN* forces are necessary for the folding calculation. We discuss now the choice of $v_{\rm D(EX)}(E,\rho,s)$ for the two bombarding energies of 0.8 and 1 GeV/nucleon. At these high energies, one can adopt the IA

which reduces the effective *NN* interaction approximately to that between the two nucleons in vacuum [14]. Consequently, the microscopic optical potential and inelastic form factors can be obtained by folding the g.s. and transition densities of the two colliding nuclei with an appropriate *t*-matrix parametrization of the free *NN* interaction.

In the present work, we have chosen the nonrelativistic *t*-matrix interaction which was developed by Franey and Love [13] based on experimental *NN* phase shifts at bombarding energies of 0.8 and 1 GeV. The spin- and isospin-independent direct (v_{D}) and exchange (v_{EX}) parts of the central *NN* interaction are then determined from the singlet- and triplet-even (SE and TE) and singlet- and triplet-odd (SO and TO) components of the local *t*-matrix interaction (see Table I of Ref. [13]) as

$$v_{\mathrm{D(EX)}}(s) = \frac{k_a k_A}{16}[3t_{\mathrm{TE}}(s) + 3t_{\mathrm{SE}}(s) \pm 9t_{\mathrm{TO}}(s) \pm 3t_{\mathrm{SO}}(s)]. \tag{9}$$

Here k_a and k_A are the energy-dependent kinematic modification factors of the *t*-matrix transformation [19] from the *NN* frame to the *Na* and *NA* frames, respectively. k_a and k_A were evaluated using Eq. (19) of Ref. [12]. The explicit, complex strength of the *finite-range* central *t*-matrix interaction (9) is given in terms of four Yukawas [13]. Since the medium modifications of the *NN* interaction are neglected in the IA [14], the *t*-matrix interaction (9) does not depend on the nuclear density.

B. Main steps in the calculation of σ_{I}

With properly chosen g.s. densities for the two colliding nuclei, the elastic scattering cross section and σ_{R} are obtained straightforwardly in the OM calculation using the microscopic optical potential (4)–(6). We recall that the interaction cross section σ_{I} is actually the sum of all particle removal cross sections from the projectile [1] and accounts, therefore, for all processes when the neutron and/or proton number in the *projectile* is changed. As a result, σ_{I} must be smaller than the total reaction cross section σ_{R} which includes also the cross section of inelastic scattering to excited states in both the target and projectile as well as cross section of nucleon removal from the target. At energies of several hundred MeV/nucleon, the difference between σ_{R} and σ_{I} was found to be a few percent [3,20,21] and was usually neglected to allow a direct comparison of the calculated σ_{R} with the measured σ_{I}. Since the experimental uncertainty in the measured σ_{I} is very small at the considered energies (around 1% for stable projectiles such as ^{4}He, ^{12}C, and ^{16}O [1]) neglecting the difference between σ_{R} and σ_{I} might be too rough an approximation in comparing the calculated σ_{R} with the measured σ_{I} and testing nuclear radius at the accuracy level of ±0.05 fm or less [1,22]. In the present work, we try to estimate σ_{I} as accurately as possible by subtracting from the calculated σ_{R} the total cross section of the main inelastic scattering channels; namely, we have calculated in DWIA, using the complex folded optical potential and inelastic form factors, the integrated cross sections σ_{2^+} and σ_{3^-} of inelastic scattering to the first excited 2^+ and 3^- states of ^{12}C target at 4.44 and 9.64 MeV, respectively. These states are known to have the largest cross sections in the inelastic proton and heavy ion scattering on ^{12}C at different energies. The deformation lengths used to construct transition densities (8) for the folding calculation were chosen so that the electric transition rates measured for these states are reproduced with the proton transition density as

$$B(E\lambda\uparrow) = e^2 \left| \int_0^\infty \rho_\lambda^p(r) r^{\lambda+2} dr \right|^2. \tag{10}$$

Using a realistic Fermi distribution for the g.s. density of ^{12}C (see the following section) to generate the transition densities, we obtain $\delta_2 \approx 1.54$ fm and $\delta_3 \approx 2.11$ fm which reproduce the experimental transition rates $B(E2\uparrow) \approx 41\ e^2\ \mathrm{fm}^4$ [23] and $B(E3\uparrow) \approx 750\ e^2\ \mathrm{fm}^6$ [24], respectively, via Eq. (10). Since inelastic scattering to excited states of the unstable projectile is suppressed by a much faster breakup process, σ_{I} can be approximately obtained as

$$\sigma_{\mathrm{I}} = \sigma_{\mathrm{R}} - \sigma_{\mathrm{Inel}} \approx \sigma_{\mathrm{R}} - \sigma_{2^+} - \sigma_{3^-}. \tag{11}$$

All the OM and DWIA calculations were made using the code ECIS97 [25] with the relativistic kinematics properly taken into account. At the energies around 1 GeV/nucleon the summation (1) is usually carried over up to 800–1000 partial waves to reach the full convergence of the *S*-matrix series for the considered nucleus-nucleus systems.

C. Adequacy and limitation of the folding approach

Since the measured σ_{I} have been analyzed extensively by different versions of Glauber model and its optical limit (OL) is sometimes referred to as the folding model [6,26], we find it necessary to highlight the distinctive features of the present folding approach in comparison with the OL of Glauber model before going to discuss the results of calculation.

On the level of the nucleus-nucleus optical potential (OP), the present double-folding approach evaluates OP using fully *finite-range NN* interaction and taking into account the exchange effects accurately via the Fock term in Eq. (3). Therefore, individual nucleons are allowed to scatter after the collision into unoccupied single-particle states only. Sometimes, one discusses these effects as the exchange *NN* correlation. An appropriate treatment of the exchange *NN* correlation is indispensable not only in the folding calculation of OP and inelastic form factor, but also in the Hartree-Fock (HF) calculations of nuclear matter [27] and of the finite nuclei [28].

To obtain from the double-folding model presented above the simple expression of nucleus-nucleus OP used in the OL of Glauber model one needs to make a "double-zero" approximation which reduces the complex finite-range *t*-matrix interaction (9) to a *zero-range* (purely imaginary) *NN* scattering amplitude at *zero NN angle* $t_{NN}(\theta=0^\circ)\delta(\boldsymbol{s})$ that can be further expressed through the total *NN* cross section σ_{NN}, using the optical theorem. As a result, one needs to evaluate in the OL of Glauber model only a simple folding integral over local densities of the two colliding nuclei [6]:

$$U(\boldsymbol{R}) \to V_{OL}(\boldsymbol{R}) = \frac{i\sigma_{NN}}{2} \int \rho_a(\boldsymbol{R})\rho_A(\boldsymbol{R} - \boldsymbol{r}_A)d^3r_A. \quad (12)$$

The prescription (12) is also known as the $t\rho\rho$ approximation [29] which neglects the off-shell part of the t matrix. Besides the inaccuracy caused by the use of zero-range approximation [30], the zero-angle approximation takes into account only the on-shell t-matrix at zero momentum transfer [see Eq. (3) in Ref. [12]]. Since the antisymmetrization of t_{NN} requires an accurate estimation of the NN knock-on exchange term which is strongest at *large* momentum transfers ($q > 6$ fm^{-1} at energies around 0.8 GeV [12,13]), the zero-angle approximation could strongly reduce the strength of the exchange term. A question remains, therefore, whether the NN antisymmetry is properly taken into account when one uses the empirical σ_{NN} in the Glauber folding integral (12). A similar aspect has been raised by Brandan *et al.* [31] who found that an *overestimated* absorption in the nucleus-nucleus system (by the $t\rho\rho$ model) is due to the effects of Pauli principle. To illustrate the importance of the knock-on exchange term, we have plotted in Fig. 1 the *direct* and *exchange* components of the microscopic OP for ^{6}He+^{12}C system at 790 MeV/nucleon predicted by our double-folding approach using realistic g.s. densities (see the following section) of the two colliding nuclei. One can see that the exchange term of the real OP is repulsive and much stronger than the (attractive) direct term, which makes the total real OP repulsive at all internuclear distances [see panel (a) of Fig. 1]. The exchange term of the imaginary OP is also repulsive but its relative strength is much weaker compared to that of the real OP, and the total imaginary OP remains attractive or *absorptive* at all distances. As a result, the direct part of the imaginary OP is about 10% more absorptive than the total imaginary OP [see panel (b) of Fig. 1]. The total reaction cross section predicted by the complex OP shown in Fig. 1 is $\sigma_R \approx 727$ mb. This value increases to $\sigma_R \approx 750$ mb when the exchange potential V_{EX} is omitted in the OM calculation. Consequently, the relative contribution by the exchange term in σ_R is about 3%. This difference is not small because it can lead to a difference of up to 7% in the extracted nuclear rms radii. Due to an overwhelming contribution by the exchange part of the real OP, the exchange potential affects the calculated elastic scattering cross section (see Fig. 2) much more substantially compared to σ_R, which is determined mainly by the *imaginary* OP.

We will show below a slight (but rather systematic) difference in σ_R values obtained in our approach and the OL of Glauber model that might be due to the exchange effect. We note further that the elastic S matrix is obtained in our approach rigorously from the quantal solution of the Schrödinger equation for elastic scattering wave, while the elastic S matrix used in the Glauber model is given by the eikonal approximation which neglects the second-derivative term of the same Schrödinger equation.

A common feature of the present folding approach and the OL of Glauber model is the use of single-particle nuclear densities of the projectile and target as input for the calculation, leaving out all few-body correlations to the structure model used to construct the density. This simple ansatz has been referred to as "static density approximation" [5,6]

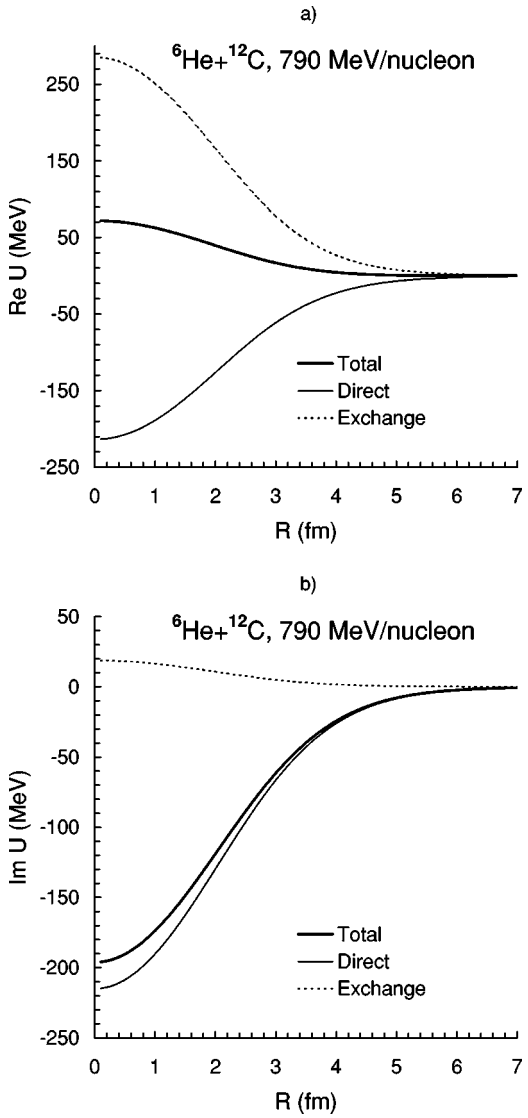

FIG. 1. Radial shape of the *direct* V_D and *exchange* V_{EX} parts of the *total* optical potential U for ^{6}He+^{12}C system at 790 MeV/nucleon. The real and imaginary part of U are shown in panels (a) and (b), respectively.

which does not take into account explicitly the dynamic few-body correlation between the core and valence nucleons in a loosely bound projectile while it collides with the target. In the Glauber model, this type of few-body correlation can be treated explicitly [3,5,6] using simple assumptions for the wave functions of the core and valence nucleons as well as that of their relative motion. For unstable nuclei with a well-extended halo structure, such as ^{11}Li or ^{6}He, such an explicit treatment of the dynamic few-body correlation leads consistently to a smaller σ_R, i.e., to a larger nuclear radius compared to that given by the OL of Glauber model [3,5,6]. On the level of the HF-type folding calculation (3), an explicit treatment of the core and valence nucleons would result in a much more complicated triple-folding formalism which involves the antisymmetrization not only between the projectile nucleons and those of the target, but also between the nucleons of the core and the valence nucleons. Such an ap-

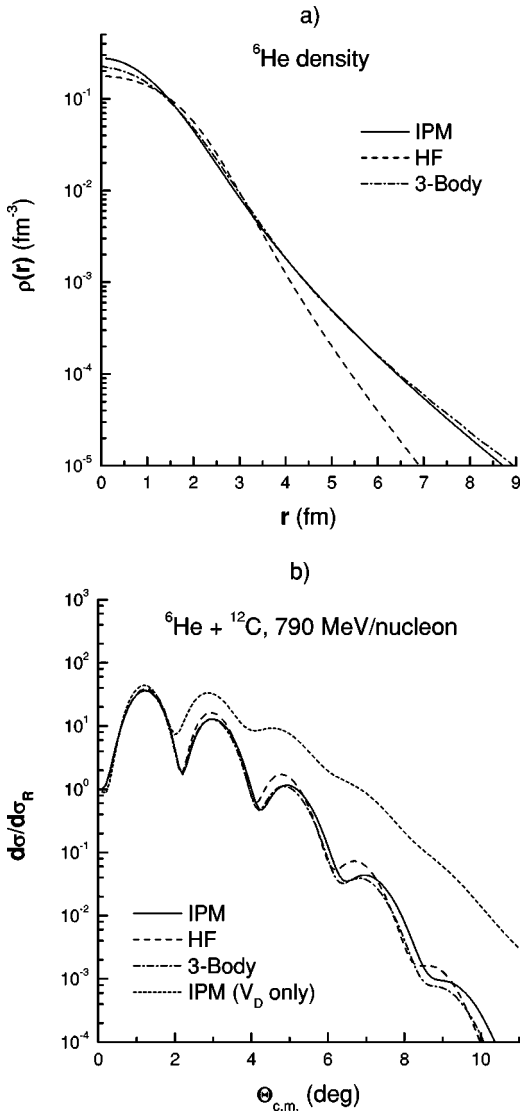

FIG. 2. Three versions of ^{6}He g.s. density used in the folding calculation [panel (a)] and elastic ^{6}He+^{12}C scattering cross sections at 790 MeV/nucleon obtained with the corresponding complex folded optical potentials [panel (b)]. The dotted curve in panel (b) is obtained without the exchange part of the OP.

proach would clearly end up with a *nonlocal* OP which will not be easily used with the existing direct reaction codes. The lack of an appropriate treatment of the dynamic few-body correlations remains, therefore, the main limitation of the present folding approach in the calculation of the OP for systems involving unstable nuclei with halo-type structure.

Note that an effective way of taking into account the loose binding between the core and valence nucleons is to add a higher-order contribution from breakup (dynamic polarization potential) to the first-order folded potential [21,32] or simply to renormalize the folded potential to fit the data. However, validity of the IA implies that higher-order multiple scattering or contribution from the dynamic polarization potential is negligible, and the folded OP and inelastic form factor based on the *t*-matrix interaction (9) should be used in the calculations without any further renormalization. Therefore, we will discuss below only results obtained with the unrenormalized folded potentials, keeping in mind possible effects due to the few-body correlation.

III. RESULTS AND DISCUSSION

A. Results for stable ($N=Z$) isotopes

An important step in any experimental or theoretical reaction study with unstable beams is to gauge the method or model by the results obtained with stable beams. Therefore, we have considered first the available data of σ_I induced by stable ^{4}He, ^{6}Li, ^{12}C, and ^{16}O beams on ^{12}C target [1]. These ($N=Z$) nuclei are strongly bound, and the rms radius of the (point) proton distribution inferred from the elastic electron scattering data [33] can be adopted as the "experimental" nuclear radius if the proton and neutron densities are assumed to be the same. To show the sensitivity of the calculated σ_I to the nuclear radius, we present in Table I results obtained with different choices for the projectile density in each case. We use for the g.s. density of ^{12}C target a realistic Fermi (FM) distribution [16]

$$\rho_0(r) = \rho_0/\{1 + \exp[(r-c)/a]\}, \tag{13}$$

where $\rho_0 = 0.194$ fm^{-3}, $c = 2.214$, and $a = 0.425$ fm were chosen to reproduce the shape of shell model density and experimental radius of 2.33 fm for ^{12}C.

^{4}He is a unique case where a simple harmonic oscillator (HO) model can reproduce quite well its ground state density. If one chooses the HO parameter to give $\langle r^2\rangle^{1/2} = 1.461$ fm (close to the experimental radius of 1.47 ± 0.02 fm), then one obtains the Gaussian form adopted in Ref. [7] for α density. This choice of ^{4}He density has been shown in the folding analysis of elastic α-nucleus scattering [16] to be the most realistic. By comparing the calculated σ_I with the data, we find that this same choice of ^{4}He density gives the best agreement between $\sigma_I^{\rm calc}$ and $\sigma_I^{\rm expt}$. Similar situation was found for ^{12}C and ^{16}O isotopes, where the best agreement with the data is given by the densities which reproduce the experimental nuclear radii. Besides a simple Fermi distribution [16], microscopic g.s. densities given by the Hartree-Fock-Bogoliubov (HFB) calculation that takes into account the continuum [34] were also used. The agreement with the data for ^{12}C and ^{16}O given by the HFB densities is around 2%, quite satisfactory for a fully microscopic structure model. We have further used *sp*-shell HO wave functions to construct the g.s. densities of ^{6}Li, ^{12}C, and ^{16}O. For ^{12}C and ^{16}O, the best agreement with the σ_I data is again reached when the HO parameter is tuned to reproduce the experimental radii.

The agreement is slightly worse for ^{6}Li compared to ^{4}He, ^{12}C, and ^{16}O cases if ^{6}Li density distribution reproduces the experimental radius. We have first used ^{6}Li density given by the independent particle model (IPM) developed by Satchler [7,35] which generates realistic wave function for each single-particle orbital using a Woods-Saxon (WS) potential for the bound state problem. The IPM density gives $\langle r^2\rangle^{1/2} \approx 2.40$ fm for ^{6}Li, rather close to the experimental radius of 2.43 ± 0.02 fm inferred from (e,e) data [33]. The HO density gives the same σ_I as that given by the IPM density if the HO

TABLE I. The total reaction cross section σ_R and interaction cross section σ_1 calculated for stable ^{4}He, ^{6,7}Li, ^{12}C, and ^{16}O nuclei in comparison with σ_I^{expt} taken from the data compilation in Ref. [1]. $\Delta\sigma_I = |\sigma_I^{calc} - \sigma_I^{expt}| / \sigma_I^{expt}$.

Nucleus	Energy (MeV/nucleon)	Density model	$\langle r^2\rangle_{calc}^{1/2}$ (fm)	Reference	$\langle r^2\rangle_{expt}^{1/2}$ (fm)	σ_R^{calc} (mb)	σ_I^{calc} (mb)	σ_I^{expt} (mb)	$\Delta\sigma_I$ (%)
^{4}He	790	HO	1.461	[7]	1.47±0.02[a]	513	504	503±5	0.2
		HO	1.550	[16]		523	515		2.4
		HO	1.720	[36]		543	536		6.6
^{6}Li	790	IPM	2.401	[35]	2.43±0.02[a]	722	717	688±10	4.2
		HO	2.401	This work		723	718		4.4
		HO	2.320	This work		709	703		2.2
^{7}Li	790	IPM	2.367	[35]	2.33±0.02[b]	746	741	736±6	0.7
		HO	2.334	This work		744	739		0.4
^{12}C	950	FM	2.332	[16]	2.33±0.02[a]	854	844	853±6	1.1
		HO	2.332	[16]		853	843		1.1
		HFB	2.446	This work		881	872		2.2
^{16}O	970	FM	2.618	[16]	2.61±0.01[a]	992	981	982±6	0.1
		HO	2.612	[16]		988	978		0.4
		HFB	2.674	This work		1006	997		1.4

[a]rms radius of the proton density given by the experimental charge density [33] unfolded with the finite size of proton.
[b]Nuclear rms radius deduced from the Glauber model analysis of the same σ_I data in the OL approximation [1].

parameter is chosen to give the same radius of 2.40 fm. These two versions of ^{6}Li density overestimate the σ_I data by about 4%. If the HO parameter is chosen to give $\langle r^2\rangle^{1/2} \approx 2.32$ fm, then the agreement with the σ_I data improves to around 2%. This result indicates that our folding + DWIA analysis slightly overestimates the absorption in ^{6}Li+^{12}C system. Since ^{6}Li is a loosely bound $\alpha+d$ system, this few percent discrepancy with the σ_I data might well be due to the dynamic correlation between the α core and deuteron cluster in ^{6}Li during the collision which is not taken into account by our approach. Note that a few-body Glauber calculation [6] (which takes into account explicitly the dynamic correlation between α and d) ends up, however, with about the same discrepancy (see Fig. 4 in Ref. [6]). ^{6}Li remains, therefore, an interesting case for the reaction models to improve their ingredients. For ^{7}Li, the IPM density [7] gives $\langle r^2\rangle_p^{1/2} \approx 2.28$ fm (close to the experimental value of 2.27±0.01 fm [33]) and $\langle r^2\rangle_n^{1/2} \approx 2.43$ fm which make the matter radius $\langle r^2\rangle^{1/2} \approx 2.37$ fm. As a result, σ_I calculated with the IPM density for ^{7}Li agrees with the data within less than 1%. In the HO model for ^{7}Li density, we have chosen the HO parameter for protons to reproduce the experimental radius of 2.27 fm and that for neutrons adjusted by the best agreement with the σ_I data. The best-fit $\langle r^2\rangle^{1/2}$ radius then becomes around 2.33 fm.

We conclude from these results that the present folding + DWIA approach and local *t*-matrix interaction by Franey and Love [13] are quite suitable for the description of the nucleus-nucleus interaction cross section at energies around 1 GeV/nucleon, with the prediction accuracy as fine as 1–2% for the stable and strongly bound nuclei.

B. Results for neutron-rich isotopes

Our results for neutron-rich He, Li, C, and O isotopes are presented in Table II. Since ^{6}He beams are now available with quite a good resolution, this nucleus is among the most studied unstable nuclei. In the present work we have tested three different choices for ^{6}He density in the calculation of σ_I. The microscopic ^{6}He density obtained in a HF calculation [30] has a rather small radius $\langle r^2\rangle^{1/2} \approx 2.20$ fm and the calculated σ_I underestimates the data by about 5%. A larger radius of 2.53 fm is given by the density obtained in a consistent three-body formalism [5] and the corresponding σ_I agrees better with the data. Given an accurate ^{7}Li density obtained in the IPM [7] as shown above and the fact that ^{6}He can be produced by a proton-pickup reaction on ^{7}Li, we have constructed the g.s. density of ^{6}He in the IPM (with the recoil effect properly taken into account [35]) using the following WS parameters for the single-particle states: $r_0 = 1.25$ fm, $a = 0.65$ fm for the $s_{1/2}$ neutrons and protons which are bound by $S_n = 25$ MeV and $S_p = 23$ MeV, respectively; $r_0 = 1.35$ fm, $a = 0.65$ fm for the $p_{3/2}$ halo neutrons which are bound by $S_n = 1.86$ MeV. The WS depth is adjusted in each case to reproduce the binding energy. The obtained IPM density gives the proton, neutron, and total nuclear radii of ^{6}He as 1.755, 2.746, and 2.460 fm, respectively. This choice of ^{6}He density also gives the best agreement with the σ_I data. We note that a Glauber model analysis of the elastic ^{6}He+p scattering at 0.7 GeV/nucleon [37], which takes into account higher-order multiple-scattering effects, gives a best-fit $\langle r^2\rangle^{1/2} \approx 2.45$ fm for ^{6}He, very close to our result. Since elastic ^{6}He+^{12}C scattering has recently been measured at lower energies [38], we found it interesting to plot the three densities and elastic ^{6}He+^{12}C scattering cross sections at 790 MeV/nucleon predicted by the corresponding complex folded OP (the radial shape of the OP obtained with the IPM density for ^{6}He is shown in Fig. 1). As can be seen from Fig. 2, the IPM density has the neutron-halo tail very close to that of the density calculated in the three-body model [5] and they both give a good description of σ_I. The

TABLE II. The same as Table I but for neutron-rich He, Li, C, and O isotopes. Note that $\langle r^2\rangle_{\rm calc}^{1/2}$ given by the HO densities should have about the same uncertainties as those deduced for $\langle r^2\rangle_{\rm expt}^{1/2}$ by the OL of Glauber model.

Nucleus	Energy (MeV/nucleon)	Density model	$\langle r^2\rangle_{\rm calc}^{1/2}$ (fm)	Reference	$\langle r^2\rangle_{\rm expt}^{1/2}$ (fm)	$\sigma_{\rm R}^{\rm calc}$ (mb)	$\sigma_{\rm I}^{\rm calc}$ (mb)	$\sigma_{\rm I}^{\rm expt}$ (mb)	$\Delta\sigma_{\rm I}$ (%)
^{6}He	790	HF	2.220	[30]	2.48±0.03[a]	691	686	722±6	5.0
		3-BODY	2.530	[5]		738	733		1.5
		IPM	2.460	This work	2.45±0.10[b]	727	722		0.0
^{8}He	790	COSMA	2.526	[39]	2.52±0.03[a]	816	812	817±6	0.6
^{8}Li	790	HO	2.371	This work	2.37±0.02[a]	782	775	768±9	0.9
^{9}Li	790	HO	2.374	This work	2.32±0.02[a]	809	802	796±6	0.7
^{11}Li	790	HO+halo	3.227	This work	3.12±0.16 [a]	1066	1061	1060±10[c]	0.1
		HF	2.868	[30]		971	967		8.8
^{13}C	960	IPM	2.389	[35]	2.28±0.04[a]	887	877	862±12	1.7
		HO	2.355	This work		875	866		0.5
^{14}C	965	HFB	2.585	This work	2.30±0.07[a]	951	941	880±19	6.9
		IPM	2.417	[35]		910	900		2.3
		HO	2.386	This work		899	888		0.9
^{15}C	740	HO	2.481	This work	2.40±0.05[a]	961	952	945±10	0.7
^{16}C	960	HFB	2.724	This work	2.70±0.03[a]	1026	1018	1036±11	1.7
		HO	2.782	This work		1039	1030		0.6
^{17}C	965	HO	2.831	This work	2.72±0.03[a]	1069	1060	1056±10	0.4
^{18}C	955	HFB	2.860	This work	2.82±0.04[a]	1102	1094	1104±15	0.9
		HO	2.900	This work		1107	1098		0.5
^{19}C	960	HO	3.238	This work	3.13±0.07[a]	1234	1227	1231±28	0.3
^{20}C	905	HFB	2.991	This work	2.98±0.05[a]	1186	1179	1187±20	0.7
		HO	3.061	This work		1196	1187		0.0
^{17}O	970	IPM	2.766	[35]	2.59±0.05[a]	1026	1016	1010±10	0.6
		HO	2.672	This work		1021	1011		0.1
^{18}O	1050	HFB	2.763	This work	2.61±0.08[a]	1053	1042	1032±26	1.0
		IPM	2.768	[35]		1057	1048		1.6
		HO	2.742	This work		1046	1036		0.4
^{19}O	970	HO	2.774	This work	2.68±0.03[a]	1076	1066	1066±9	0.0
^{20}O	950	HFB	2.849	This work	2.69±0.03[a]	1122	1112	1078±10	3.1
		HO	2.786	This work		1100	1089		1.0
^{21}O	980	HO	2.811	This work	2.71±0.03[a]	1116	1105	1098±11	0.6
^{22}O	965	HFB	2.919	This work	2.88±0.06[a]	1170	1159	1172±22	1.1
		HO	2.956	This work		1178	1168		0.3
^{23}O	960	HO	3.286	This work	3.20±0.04[a]	1310	1302	1308±16	0.5
^{24}O	965	HFB	3.050	This work	3.19±0.13[a]	1248	1238	1318±52	6.1
		HO	3.280	This work		1319	1311		0.5

[a]Nuclear rms radius deduced from the Glauber model analysis of the $\sigma_{\rm I}$ data in the OL approximation [1].
[b]Nuclear rms radius deduced from the Glauber model analysis of elastic ^{6}He+p scattering data at 0.7 GeV/nucleon [37].
[c]$\sigma_{\rm I}$ data taken from Ref. [41].

predicted elastic cross section is strongly forward peaked and the difference in densities begins to show up after the first diffractive maximum. Such a measurement should be feasible at the facilities used for elastic ^{6}He+p scattering at 0.7 GeV/nucleon [37] and would be very helpful in testing finer details of ^{6}He density. As already discussed in the preceding section, the exchange part of the microscopic OP affects the elastic cross section very strongly [see dotted curve in panel (b) of Fig. 2] and the elastic ^{6}He+^{12}C scattering measurement would be also a very suitable probe of the exchange effects in this system.

Since ^{6}He is a loosely bound halo nucleus with a well established three-body $\alpha+n+n$ structure, the dynamic correlation between the α core and dineutron is expected to be important during the collision. Our folding + DWIA approach using three-body density for ^{6}He (version FC [5]) gives $\sigma_{\rm I}\approx 733$ mb compared to about 720 mb given by the few-body calculation by Tostevin *et al.* (see Fig. 4 in Ref.

TABLE III. The HO-density parameters (14) for neutron-rich Li, C, and O isotopes.

Nucleus	P_n	P_p	D_n	D_p	b_n (fm)	b_p (fm)	$\langle r^2\rangle_n^{1/2}$ (fm)	$\langle r^2\rangle_p^{1/2}$ (fm)	$\langle r^2\rangle^{1/2}$ (fm)
^{7}Li	2/3	1/3	0.0	0.0	1.684	1.6766	2.382	2.270	2.334
^{8}Li	1.0	1/3	0.0	0.0	1.6770	1.6776	2.430	2.270	2.371
^{9}Li	4/3	1/3	0.0	0.0	1.6470	1.6766	2.424	2.270	2.374
^{13}C	5/3	4/3	0.0	0.0	1.6058	1.5722	2.389	2.314	2.355
^{14}C	2.0	4/3	0.0	0.0	1.6226	1.5762	2.434	2.320	2.386
^{15}C	2.0	4/3	2/15	0.0	1.6630	1.5898	2.570	2.340	2.481
^{16}C	2.0	4/3	4/15	0.0	1.8512	1.7128	2.927	2.521	2.782
^{17}C	2.0	4/3	2/5	0.0	1.8552	1.7128	2.986	2.521	2.831
^{18}C	2.0	4/3	8/15	0.0	1.8752	1.7297	3.062	2.546	2.900
^{19}C	2.0	4/3	2/3	0.0	2.1252	1.7297	3.512	2.546	3.238
^{20}C	2.0	4/3	4/5	0.0	1.9462	1.7467	3.248	2.571	3.061
^{17}O	2.0	2.0	2/15	0.0	1.7775	1.7232	2.747	2.585	2.672
^{18}O	2.0	2.0	4/15	0.0	1.7601	1.7935	2.783	2.690	2.742
^{19}O	2.0	2.0	2/5	0.0	1.7601	1.7935	2.833	2.690	2.774
^{20}O	2.0	2.0	8/15	0.0	1.7401	1.8005	2.842	2.701	2.786
^{21}O	2.0	2.0	2/3	0.0	1.7401	1.8005	2.876	2.701	2.811
^{22}O	2.0	2.0	4/5	0.0	1.8498	1.8081	3.087	2.712	2.956
^{23}O	2.0	2.0	14/15	0.0	2.1118	1.8081	3.555	2.712	3.286
^{24}O	2.0	2.0	16/15	0.0	2.0758	1.8261	3.520	2.739	3.280

[6]) based on the same three-body wave function for ^{6}He. The difference in the calculated $\sigma_{\rm I}$ leads to an increase of about 2–3% in the $\langle r^2\rangle^{1/2}$ value. It is likely that such a difference is, in part, due to the dynamic correlation between the α core and dineutron which was not considered in our folding + DWIA approach. For ^{8}He nucleus, the OL of Glauber analysis of $\sigma_{\rm I}$ data [1], and the multiple-scattering Glauber analysis of elastic ^{8}He+p data at 0.7 GeV/nucleon [38] give $\langle r^2\rangle^{1/2}$ around 2.52 and 2.53 fm, respectively. By using the microscopic ^{8}He density obtained in a four-body (COSMA) model [39], which gives $\langle r^2\rangle^{1/2}=2.526$ fm, our folding + DWIA approach reproduces the measured $\sigma_{\rm I}$ data within less than 1%. Note that a (multiple scattering) Glauber model analysis of the elastic ^{6,8}He+p scattering at 0.7 GeV/nucleon which takes into account the dynamic few-body correlation explicitly was done by Al-Khalili and Tostevin [40], and they have obtained the best-fit nuclear radii of about 2.5 and 2.6 fm for ^{6}He and ^{8}He, respectively, around 2% larger than our results.

1. Parameters of HO densities deduced from $\sigma_{\rm I}$ data

Although the HO model is a very simple approach, the HO densities were shown above to be useful in testing the nuclear radii for stable ($N=Z$) nuclei. Moreover, the HO-type densities (with the appropriately chosen HO lengths) for the *sd*-shell nuclei have been successfully used in the analysis of (e,e) data, measurements of isotope shift, and muonic atoms [1]. Therefore, it is not unreasonable to use simple HO parametrization for the g.s. densities of neutron-rich nuclei to estimate the nuclear radii, based on our folding + DWIA analysis of $\sigma_{\rm I}$ data. For a $N\neq Z$ nucleus, one needs to generate proton and neutron densities separately as

$$\rho_\tau(r)=\frac{2}{\pi^{3/2}b_\tau^3}\left(1+P_\tau\frac{r^2}{b_\tau^2}+D_\tau\frac{r^4}{b_\tau^4}\right)\exp\left(-\frac{r^2}{b_\tau^2}\right), \qquad (14)$$

where $\tau=n$ or p, parameters P_τ and D_τ are determined from the nucleon occupation of the p and d harmonic oscillator shells, respectively.

To generate the g.s. densities of ^{8,9}Li isotopes, we have assumed the proton density of these nuclei to be approximately that of ^{7}Li and the neutron HO length b_n is adjusted in each case to reproduce the measured $\sigma_{\rm I}$ (see Tables II and III). While the obtained $\langle r^2\rangle^{1/2}$ for ^{8}Li is rather close to that given by the OL of Glauber model [1], results obtained for ^{9}Li are different and we could reproduce the $\sigma_{\rm I}$ data only if the neutron HO length is chosen to give $\langle r^2\rangle_{\rm calc}^{1/2}\approx 2.37$ fm or about 2% larger than that given by the OL of Glauber model. For the halo nucleus ^{11}Li, a ^{9}Li core + two-neutron halo model was used to generate its density; namely, we have used HO density of ^{9}Li that reproduces the measured $\sigma_{\rm I}$ for ^{9}Li and a Gaussian tail for the two-neutron halo density. To reach the best agreement between $\sigma_{\rm I}^{\rm expt}$ taken from Ref. [41] and $\sigma_{\rm I}^{\rm calc}$, the Gaussian range was chosen to give $\langle r^2\rangle_{\rm calc}^{1/2}\approx 3.23$ fm which is about 0.1 fm larger than that given by the OL of Glauber model [1]. A microscopic density for ^{11}Li obtained in the HF calculation [30] (which gives $\langle r^2\rangle^{1/2}=2.868$ fm) has also been used in our folding analysis. The agreement with the data becomes much worse in this case (see Table II) and we conclude that the radius given by the HF density is somewhat too small. To show the sensitivity of

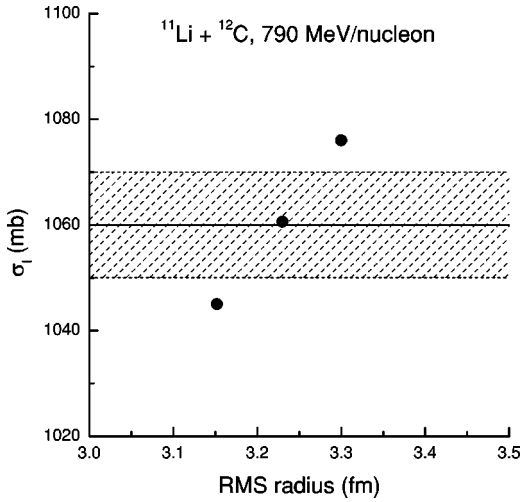

FIG. 3. σ_I^{calc} obtained with three versions of ^{11}Li g.s. density, where Gaussian range of the 2*n*-halo was adjusted to give $\langle r^2\rangle^{1/2}$ = 3.15, 3.23, and 3.30 fm for ^{11}Li, in comparison with σ_I^{expt} = 1060 ± 10 mb [41].

our analysis to the nuclear radius, we have plotted in Fig. 3 σ_I predicted by three versions of ^{11}Li density with the Gaussian range of the 2*n*-halo adjusted to give $\langle r^2\rangle^{1/2}$ = 3.15, 3.23, and 3.30 fm, respectively, compared to σ_I^{expt} = 1060 ± 10 mb [41]. It is easily to infer from Fig. 3 an empirical rms radius of 3.23 ± 0.05 fm for ^{11}Li. Note that σ_I measurement for ^{11}Li+^{12}C system at 790 MeV/nucleon has been reported in several works with σ_I^{expt} = 1040 ± 60 [42], 1047 ± 40 [43], and 1060 ± 10 mb [41]. If we adjust Gaussian range of the 2*n*-halo in ^{11}Li density to reproduce these σ_I^{expt} values, the corresponding $\langle r^2\rangle^{1/2}$ radii of ^{11}Li are 3.13, 3.15, and 3.23 fm, respectively. Since σ_I data obtained in Ref. [41] have a much better statistics and less uncertainty, we have adopted $\langle r^2\rangle^{1/2}$ = 3.23 ± 0.05 fm as the most realistic rms radius of ^{11}Li given by our folding + DWIA analysis.

The total reaction cross section for ^{11}Li+^{12}C system at 790 MeV/nucleon has been studied earlier in the few-body Glauber formalism by Al-Khalili *et al.* [5], where $\langle r^2\rangle^{1/2}$ radius for ^{11}Li was shown to increase from 3.05 fm (in the OL) to around 3.53 fm when the dynamic correlation between ^{9}Li-core and 2*n*-halo during the collision is treated explicitly. This is about 9% larger than $\langle r^2\rangle^{1/2}$ radius obtained in our folding + DWIA approach based on the same σ_I data. Although various structure calculations for ^{11}Li give its rms radius around 3.1–3.2 fm (see Refs. [1,4] and references therein), a very recent coupled-channel three-body model for ^{11}Li by Ikeda *et al.* [44,45] shows that its rms radius is ranging from 3.33 to 3.85 fm if the 2*n*-halo wave function consists of 21–39% mixture from $(s_{1/2})^2$ state, respectively. A comparison of the calculated Coulomb breakup cross section with the data [45] suggests that this *s*-wave mixture is around 20–30%. Thus, the nuclear radius of ^{11}Li must be larger than that accepted so far [1,4] and be around 3.3–3.5 fm, closer to the result of the few-body calculation [5] and the upper limit of rms radius given by our folding + DWIA analysis.

For most of neutron-rich C and O isotopes considered here, we have first fixed the proton HO lengths b_p to reproduce the proton $\langle r^2\rangle_p^{1/2}$ radii predicted by the microscopic IPM and HFB densities (as described below). The neutron HO lengths b_n are then adjusted to the best agreement with σ_I data, and the obtained HO parameters are summarized in Table III.

2. Microscopic HFB densities

Before discussing the results obtained for the neutron-rich C and O isotopes, we give here a brief description of the microscopic HFB approach used to calculate the g.s. densities of even C and O isotopes. More details about this approach can be found in Ref. [34].

We solve the HFB equations in coordinate representation and in spherical symmetry with the inclusion of continuum states for neutron-rich nuclei. As the neutron Fermi energies of these nuclei are typically quite close to zero, pairing correlations can easily scatter pairs of neutrons from the bound states towards continuum states. For this reason, the inclusion and the treatment of continuum states in the calculation are very important. In our calculation the continuum is treated exactly, i.e., with the correct boundary conditions for continuum wave functions and by taking into account the widths of the resonances. Resonant states are localized by studying the behavior of the phase shifts with respect to the quasiparticle energy for each partial wave (l,j).

The calculations were done with the Skyrme interaction SLy4 for the mean field channel and with the following zero-range density-dependent interaction

$$V = V_0\left[1 - \left(\frac{\rho(r)}{\rho_0}\right)^{\gamma}\right]\delta(\mathbf{r}_1 - \mathbf{r}_2) \qquad (15)$$

for the pairing channel. In Eq. (15), ρ_0 is the saturation density and γ is chosen equal to 1. We have adapted the prescription of Refs. [46,47] to finite nuclei in order to fix V_0 together with the quasiparticle energy cutoff. This prescription, requiring that the free neutron-neutron scattering length has to be reproduced in the truncated space, allows us to deduce a relation between the parameter V_0 and the quasiparticle energy cutoff.

3. Nuclear radii of carbon and oxygen isotopes

The σ_I data for neutron-rich C and O isotopes are compared in Table II with σ_I predicted by different choices of nuclear densities. We have tested first the IPM density for ^{13}C [35] based on the single-particle spectroscopic factors obtained in the shell model by Cohen and Kurath [48]. This IPM density gives $\langle r^2\rangle^{1/2} \approx 2.39$ fm for ^{13}C and the predicted σ_I agrees with the data within less than 2%. We have further made IPM calculation for ^{14}C based on the same single-particle configurations, with the WS parameters for *sp* shells appropriately corrected for the recoil effects and experimental nucleon separation energies $S_{n,p}$ of ^{14}C. This IPM density gives $\langle r^2\rangle^{1/2} \approx 2.42$ fm for ^{14}C and the predicted σ_I also agrees with the data within 2%. The HO densities were also parametrized for ^{13,14}C with the proton HO lengths b_p chosen to reproduce $\langle r^2\rangle_p^{1/2}$ values predicted by the IPM. The best-fit neutron HO lengths b_n result in $\langle r^2\rangle^{1/2}$ = 2.36 and 2.39 fm for

^{13}C and ^{14}C, respectively. These values agree fairly with those given by the IPM densities. The microscopic HFB density gives for ^{14}C a significantly larger $\langle r^2\rangle^{1/2}$ radius of 2.59 fm and the calculated σ_I overestimates the data by nearly 7%. Note that the OL of Glauber model gives smaller radius of 2.28 and 2.30 fm for ^{13}C and ^{14}C, respectively, based on the same σ_I data [1]. This means that the absorption given by the OL of Glauber model is indeed stronger than that given by our approach, as expected from discussion in Sec. II.

For the neutron-rich even $^{16-20}$C isotopes, the HFB densities give a remarkably better agreement with the data and it is, therefore, reasonable to fix the proton HO lengths of the HO densities for each of $^{15-20}$C isotopes to reproduce $\langle r^2\rangle_p^{1/2}$ radius predicted by the HFB calculation for the nearest even neighbor. The best-fit neutron HO lengths result in the nuclear radii quite close to those given by the HFB densities (see Tables II and III). We emphasize that the nuclear radii given by our analysis, using the HO densities for C isotopes, are about 0.1 fm larger than those deduced from the OL of Glauber model [1]. Given a high sensitivity of σ_I data to the nuclear size, a difference of 0.1 fm is not negligible.

To illustrate the mass dependence of the nuclear radius, we have plotted in Fig. 4(a) the rms radii given by the two sets (HFB and HO) of the g.s. densities for C isotopes together with those deduced from the OL of Glauber model based on the same σ_I data [1]. One can see that our result follows closely the trend established by the OL of Glauber model, although the absolute $\langle r^2\rangle^{1/2}$ radii obtained with the HO densities are in most cases larger than those deduced from the OL of Glauber model. With the exception of the ^{14}C case, the radii of even C isotopes given by the microscopic HFB densities agree reasonably well with the empirical HO results. We have also plotted in Fig. 4 the lines representing $r_0A^{1/3}$ dependence with r_0 deduced from the experimental radii of ^{12}C and ^{16}O given in Table I. One can see that the behavior of nuclear radius in C isotopes is quite different from the $r_0A^{1/3}$ law. While $\langle r^2\rangle^{1/2}$ radii found for $^{12-15}$C agree fairly with the $r_0A^{1/3}$ law, those obtained for $^{16-20}$C are significantly higher. In particular, a jump in the $\langle r^2\rangle^{1/2}$ value was found in ^{16}C compared to those found for $^{12-15}$C. This result seems to support the existence of a neutron halo in ^{16}C as suggested from the σ_R measurement for this isotope at 85 MeV/nucleon [49]. We have further obtained a nuclear radius of 3.24 fm for ^{19}C which is significantly larger than that found for ^{20}C. This result might also indicate to a neutron halo in this odd C isotope.

Situation is a bit different for O isotopes, where the best-fit $\langle r^2\rangle^{1/2}$ radii follow roughly the $r_0A^{1/3}$ law up to ^{22}O. For the stable ^{17,18}O isotopes, the IPM densities [35] provide a very good description of the σ_I data (within 1–2%). The best-fit HO densities give $\langle r^2\rangle^{1/2}$ radii of 2.67 and 2.74 fm for ^{17}O and ^{18}O, respectively, which are rather close to those given by the IPM densities. Predictions given by the microscopic HFB densities are also in a good agreement with the data for even O isotopes excepting the ^{24}O case, where the HFB density gives obviously a too small $\langle r^2\rangle^{1/2}$ radius. Since the HFB calculation already takes into account the continuum effects [34], such a deficiency might be due to the static deformation of ^{24}O. A jump in the $\langle r^2\rangle^{1/2}$ value was found for ^{23}O which could indicate to a neutron halo in this isotope. Behavior of $\langle r^2\rangle^{1/2}$ radii given by the best-fit HO densities agrees with the trend established by the OL of Glauber model [1] but, like the case of C isotopes, they are about 0.1 fm larger than those deduced from the OL of Glauber model. Thus, the OL of Glauber model seems to consistently overestimate σ_R for the neutron-rich C and O isotopes under study in comparison with our approach.

One clear reason for the difference between our results and those given by the OL of Glauber model analysis is that one has matched directly the calculated σ_R with the measured σ_I in the Glauber model analysis [1] to deduce the nuclear radius. If we proceed the same way with the HO

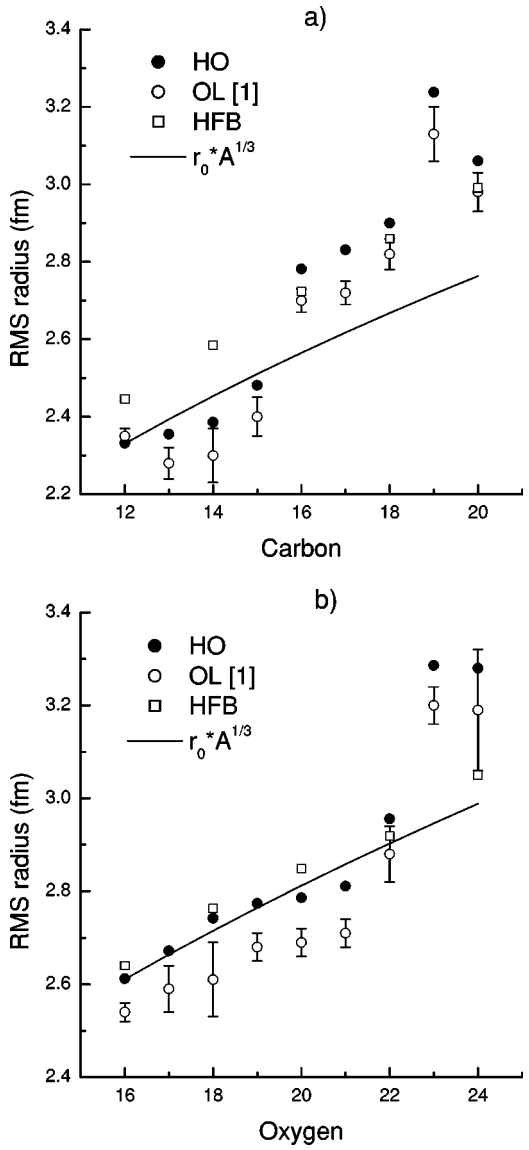

FIG. 4. Mass dependence of the nuclear rms radius for carbon [panel (a)] and oxygen [panel (b)] isotopes given by the two choices (HFB and HO) of the g.s. densities compared to that deduced from the Glauber model analysis in the OL approximation [1]. The lines represent $r_0A^{1/3}$ dependence with r_0 deduced from the experimental radii of ^{12}C and ^{16}O given in Table I.

densities for the considered nuclei, the best-fit $\langle r^2\rangle^{1/2}$ radii decrease slightly but are still larger than those given by the OL of Glauber model. As already discussed in Sec. II, the zero-angle approximation for the *NN* scattering amplitude used in the Glauber model might reduce significantly the strength of the exchange part of the imaginary OP given by Eq. (12) and could overestimate, therefore, the absorption in the dinuclear system. This effect should be much stronger if one uses a realistic finite-range representation of the *NN* scattering amplitude. Bertsch *et al.* have shown [30] that the zero-range approximation for the *NN* scattering amplitude leads to a reduction of the calculated σ_R or an enhancement of the nuclear radius by a few percent (see Figs. 2 and 3 in Ref. [30]). Owing to such a cancellation of the exchange effects by the zero-range approximation for *NN* scattering amplitude, the simple OL of Glauber model was able to deliver reasonable estimates of nuclear radii for many stable and unstable isotopes [1]. It should be noted that the eikonal approximation for the scattering wave function used in the Glauber model was introduced in the past to avoid large numerical calculations. With the computing power available today, there is no problem to perform the OM and DWIA calculations for different nucleus-nucleus systems involving large numbers of partial waves, and the folding + DWIA method presented here can be recommended as a reliable microscopic approach to predict the elastic scattering cross section and to deduce the nuclear radius from the measured σ_I.

IV. CONCLUSION

In this work we have explored the reliability of the optical model + DWIA approach as a tool for extracting important information on nuclear sizes from interaction cross section measurements. We concentrate on the energy region of 0.8–1 GeV/nucleon where interaction cross section data exist for various combinations of stable as well as unstable projectiles on different targets. At these bombarding energies our knowledge of the empirical optical potential is scarce, especially for unstable systems, and we have used, therefore, the folding model to calculate the microscopic (complex) optical potential and inelastic form factors necessary for our analysis.

We have chosen for the folding input the fully finite-range *t*-matrix interaction developed by Franey and Love [13]. The folded optical potentials and inelastic form factors are used further as inputs for the standard optical model and DWIA calculations of total reaction cross sections and interaction cross sections induced by stable and unstable He, Li, C, and O isotopes on ^{12}C target. By using the well tested nuclear g.s. densities for the stable ^{4}He, ^{12}C, and ^{16}O isotopes, we found that the Franey and Love *t* matrix gives extremely good account of the measured σ_I for these nuclei.

We have further used the nuclear g.s. densities obtained in various structure models to calculate σ_I and have made realistic estimate for the nuclear radii of (still poorly known) neutron-rich isotopes based on the comparison between σ_I^{calc} and σ_I^{expt}. For the chains of C and O isotopes, our results agree reasonably well with the empirical trend established by the OL of Glauber model [1], but give consistently larger $\langle r^2\rangle^{1/2}$ radii for these nuclei. Such an effect could be due to the unsatisfactory treatment of the exchange part of the nucleus-nucleus OP in the Glauber model calculation.

Although the nuclear radii deduced by our approach for some light halo nuclei might be a few percent smaller than realistic values because the dynamic few-body correlation was not considered explicitly in the present folding + DWIA formalism, this fully microscopic approach was shown to be more accurate than the OL of Glauber model. Given realistic nuclear densities, it can give a reliable (parameter-free) prediction of the nucleus-nucleus optical potential at energies around 1 GeV/nucleon. Therefore, it provides the necessary link to relate the calculated σ_I to the nuclear density and rms radius.

ACKNOWLEDGMENTS

The authors thank G. R. Satchler for making the DOLFIN code available to them for the IPM calculation of nuclear g.s. densities, W. von Oertzen for helpful discussion, and W. G. Love for critical remarks to the manuscript. We also thank A. Ozawa, H. Sagawa, and I. J. Thompson for their correspondence on the nuclear densities. The research has been supported, in part, by the Natural Science Council of Vietnam.

[1] A. Ozawa, T. Suzuki, and I. Tanihata, Nucl. Phys. **A693**, 32 (2001).
[2] R. J. Glauber and G. Matthiae, Nucl. Phys. **B21**, 135 (1970).
[3] Y. Ogawa, K. Yabana, and Y. Suzuki, Nucl. Phys. **A543**, 722 (1992).
[4] I. Tanihata, J. Phys. G **22**, 157 (1996).
[5] J. S. Al-Khalili, J. A. Tostevin, and I. J. Thompson, Phys. Rev. C **54**, 1843 (1996).
[6] J. A. Tostevin, R. C. Johnson, and J. S. Al-Khalili, Nucl. Phys. **A630**, 340c (1998).
[7] G. R. Satchler and W. G. Love, Phys. Rep. **55**, 183 (1979).
[8] Dao T. Khoa, G. R. Satchler, and W. von Oertzen, Phys. Rev. C **56**, 954 (1997).
[9] G. Bertsch, J. Borysowicz, H. McManus, and W. G. Love, Nucl. Phys. **A284**, 399 (1977); N. Anantaraman, H. Toki, and G. F. Bertsch, *ibid.* **A398**, 269 (1983).
[10] Dao T. Khoa and G. R. Satchler, Nucl. Phys. **A668**, 3 (2000).
[11] Dao T. Khoa, G. R. Satchler, and N. D. Thuy, Phys. Rev. C **65**, 024611 (2002).
[12] W. G. Love and M. A. Franey, Phys. Rev. C **24**, 1073 (1981).
[13] M. A. Franey and W. G. Love, Phys. Rev. C **31**, 488 (1985).
[14] G. R. Satchler, *Direct Nuclear Reactions* (Clarendon, Oxford, 1983).
[15] B. Sinha, Phys. Rep. **20**, 1 (1975); B. Sinha and S. A. Mosz-

kowski, Phys. Lett. **81B**, 289 (1979).
[16] Dao T. Khoa, Phys. Rev. C **63**, 034007 (2001).
[17] M. E. Farid and G. R. Satchler, Phys. Lett. **146B**, 389 (1984).
[18] A. Bohr and B. R. Mottelson, *Nuclear Structure* (Benjamin, New York, 1975), Vol. 2.
[19] A. K. Kerman, H. McManus, and R. M. Thaler, Ann. Phys. (N.Y.) **8**, 551 (1959).
[20] J. Jaros *et al.*, Phys. Rev. C **18**, 2273 (1978).
[21] Dao T. Khoa, G. R. Satchler, and W. von Oertzen, Phys. Lett. B **358**, 14 (1995).
[22] A. Ozawa *et al.*, Nucl. Phys. **A691**, 599 (2001).
[23] S. Raman, C. W. Nestor, Jr., and P. Tikkanen, At. Data Nucl. Data Tables **78**, 1 (2001).
[24] R. H. Spear, At. Data Nucl. Data Tables **42**, 55 (1989).
[25] J. Raynal, *Computing as a Language of Physics* (IAEA, Vienna, 1972), p. 75; computer code ECIS97 (unpublished).
[26] H. Esbensen and G. F. Bertsch, Phys. Rev. C **59**, 3240 (1999).
[27] Dao T. Khoa and W. von Oertzen, Phys. Lett. B **304**, 8 (1993); **342**, 6 (1995).
[28] H. Nakada, Phys. Rev. C **68**, 014316 (2003).
[29] M. S. Hussein, R. A. Rego, and C. A. Bertulani, Phys. Rep. **201**, 279 (1991).
[30] G. F. Bertsch, B. A. Brown, and H. Sagawa, Phys. Rev. C **39**, 1154 (1989); H. Sagawa (private communication).
[31] M. E. Brandan, H. Chehime, and K. W. McVoy, Phys. Rev. C **55**, 1353 (1997).
[32] Dao T. Khoa, G. R. Satchler, and W. von Oertzen, Phys. Rev. C **51**, 2069 (1995).
[33] H. De Vries, C. W. De Jager, and C. De Vries, At. Data Nucl. Data Tables **36**, 503 (1987).
[34] M. Grasso, N. Sandulescu, N. Van Giai, and R. J. Liotta, Phys. Rev. C **64**, 064321 (2001).
[35] G. R. Satchler, Nucl. Phys. **A329**, 233 (1979).
[36] V. B. Soubbotin and X. Viñas, J. Phys. G **25**, 2087 (1999); Nucl. Phys. **A665**, 291 (2000).
[37] G. D. Alkhazov *et al.*, Nucl. Phys. **A712**, 269 (2002).
[38] V. Lapoux *et al.*, Phys. Rev. C **66**, 034608 (2002).
[39] M. V. Zhukov, A. A. Korsheninnikov, and M. H. Smedberg, Phys. Rev. C **50**, R1 (1994).
[40] J. S. Al-Khalili and J. A. Tostevin, Phys. Rev. C **57**, 1846 (1998).
[41] T. Kobayashi *et al.*, Phys. Lett. B **232**, 51 (1989).
[42] I. Tanihata *et al.*, Phys. Rev. Lett. **55**, 2676 (1985).
[43] I. Tanihata *et al.*, Phys. Lett. B **206**, 592 (1988).
[44] K. Ikeda, T. Myo, and K. Kato, Nucl. Phys. **A722**, 335c (2003).
[45] T. Myo, S. Aoyama, K. Kato, and K. Ikeda, Phys. Lett. B **576**, 281 (2003).
[46] E. Garrido, P. Sarriguren, E. Moya de Guerra, and P. Schuck, Phys. Rev. C **60**, 064312 (1999).
[47] G. F. Bertsch and H. Esbensen, Ann. Phys. (N.Y.) **209**, 327 (1991).
[48] S. Cohen and D. Kurath, Nucl. Phys. **A101**, 1 (1967).
[49] T. Zheng *et al.*, Nucl. Phys. **A709**, 103 (2002).